Structural and defect changes in black carbon charcoal irradiated with gamma ray

K.S. Almugren [a], S.F. Abdul Sani [b,*], Irzwan Affendy Sulong [b], S.N. Mat Nawi [c,d], A.S. Siti Shafiqah [e], D.A. Bradley [c,f]

[a] Department of Physics, Princess Nourah Bint Abdulrahman University, Riyadh, Saudi Arabia
[b] Department of Physics, Faculty of Science, University of Malaya, 50603, Kuala Lumpur, Malaysia
[c] Centre for Applied Physics and Radiation Technologies, School of Engineering and Technology, Sunway University, 47500, Bandar Sunway, Selangor, Malaysia
[d] Department of Medical Sciences, School of Medical and Life Sciences, Sunway University, 47500, Bandar Sunway, Selangor, Malaysia
[e] Department of Physics, Kuliyyah of Science, International Islamic University Malaysia, 25200, Kuantan, Malaysia
[f] Department of Physics, University of Surrey, Guildford, GU2 7XH, UK

ARTICLE INFO

ABSTRACT

This study investigates the use of black carbon charcoal as passive radiation dosimetry, offering low dependence on photon energy and near soft tissue effective atomic number with state-of-the-art techniques. Regression analyses have now been conducted using graphite manufactured commercially in the form of charcoal from three different types: mangrove, coconut, and green charcoal recycled from sawdust, working with photon-mediated interactions at radiotherapy dose levels. Explorations of changes in Raman spectroscopic characteristics, and photoluminescence dose dependence have been performed with a focus on the relationship between absorbed radiation energy and induced material changes, using a ^{60}Co gamma-ray source doses ranging from 0 to 10 Gy. Raman spectroscopy has established to be an effective method for exploring defects in carbon-based materials due to its high sensitivity, most commonly focusing on the use of I_D/I_G parameter. While photoluminescence analysis will provide information on electronic properties and the band gap energy. The crystal structure of the black charcoal samples was characterised using X-ray diffractometry, with the goal of determining the degree of structural order, atomic spacing, and lattice constants of the various irradiated charcoal samples, supported by crystallite size assessments. The findings of this study could pave the way for a low-cost yet highly effective system for studying radiation-induced changes in carbon, as well as offering a viable alternative to current commercial dosimeters, well suited to applications in radiotherapy.

1. Introduction

Carbon-based materials such as graphite, charcoal, and carbon black have been used as writing and drawing materials ever since prehistoric times. Recently, carbon-rich materials have found use in a variety of fields, including electronics, sensors, composite materials, energy storage and conversion, medical application and so on due to good electrical/thermal conductivity, low density, excellent corrosion resistance, and reinforcing capability (Arora et al., 2014). Charcoal-based preparations have also been used in a variety of medical applications, most notably as an antidote for acute poisoning and drug overdose, and less frequently for the treatment of skin infections, wound malodor and pruritus associated with dialysis, as a drug nanocarrier, and medical

tattooing (Brooks et al., 2017).

Charcoal is a light black carbon residue made by rapidly heating wood (or other animal and plant materials) in a low-oxygen environment to remove all water and volatile components. Also called the organic rocks i.e., lithified plant remains composed of igneous and metamorphic rocks that were established during the Carboniferous Period. Charcoal comes in a variety of types, including: (i) Common charcoal is made from coal, peat, coconut shell or wood; (ii) Lump charcoal is a type of traditional charcoal that is made entirely of hardwood; (iii) Activated carbon, also known as activated charcoal, is a type of carbon that is processed (activated) to have small, low-volume pores that increase the surface area available for adsorption or chemical reactions; and (iv) Sawdust briquette charcoal is created by compressing

sawdust without the use of binders or admixtures, which has a round hole through the core with a hexagonal intersection. In this context, some types of charcoals i.e. mangrove, coconut and sawdust charcoals appear to offer a convenient platform for studying irradiation effects and their potential in radiation dosimetry in the dose regime of current interest, focusing on the relationship between absorbed radiation energy and induced material changes.

Thus, the novel goal of this study is to look into low linear energy transfer (0.2 keV) irradiations for various types of black carbon charcoal using ^{60}Co gamma rays in order to focus on medical applications of ionizing radiation as a passive radiation sensor, due to lower cost carbon-based material, low dependence on photon energy and has an effective atomic number (Z_{eff}) equivalent to human soft tissue (7.4). The latter is in accordance with previous carbon studies by the member of groups, focusing on the use of other carbon-rich materials (pencil, hair etc) for radiotherapy dose regime applications, examining the structural changes induced by sample formation and ionizing radiation (Lam et al., 2021; Bradley et al., 2021; Nawi et al., 2020, 2021; Abdul Sani et al., 2020). Most prominently, immediate apparent is that readily available charcoal samples can serve as the foundation for a low-cost yet highly effective system for studying radiation-driven changes in carbon-based composites, as well as a dosimetric probe of skin dose, with its an effective atomic number (Z_{eff}) similar to that of human soft tissue, pointing to favourable measurement of dose deposited in the human body.

The current study focuses on the structural changes of irradiated black carbon charcoal, determining details on the physical parameters of defects involved in the luminescence process when subjected to gamma rays within the range 0–10 Gy, a range of particular importance in radiotherapeutic applications. Raman and Photoluminescence (PL) spectroscopy were used in the study as state-of-the-art technology for carbon-based materials. Calculation of the bandgap energy and crystal size of charcoal have also been determined. Another aspect of the present work is the identification of the effective atomic number of charcoals, which is accomplished through elemental composition analysis using SEM-EDX method. Finally, X-ray diffraction (XRD) will be used to study the interlayer spacing and the crystallinity of charcoal samples. The findings of this investigation are expected to lead to sensitive, high precision radiation dosimeters for use as passive radiation dosimeters in radiation physics.

2. Material and method

2.1. Samples preparation and irradiation

Investigation has been made of three different commercially charcoal types: mangrove, coconut, and green charcoal recycled from sawdust (directly available from manufacturers, JS Resources Pte Ltd) (see Fig. 1). Using a stainless-steel knife, the charcoal samples were cut into squares measuring approximately 0.5 × 0.5 × 0.1 cm. Prior to irradiation, using a programmable furnace (Micro-controller X; model

PXR4/5/7/9) the charcoal samples were annealed for a period of 1 h at a temperature of 400 °C to removed the evidence of any prior electron-hole trapping or natural irradiation history (e.g., from background radiation and mechanical strain), then cooled down under natural or unforced conditions to minimize any propensity for thermal stress and with it the potential for additional defects generation (Nawi et al., 2021). Irradiations were made, delivering doses ranging from 2 to 10 Gy at a dose rate of 1.09 Gy/min using a ^{60}Co gamma irradiator (mean energy 1.25 MeV), manufactured by Atomic Energy Canada Limited, located at the Department of Physics, University of Malaya. The samples were placed in the centre of the chamber to ensure that all samples received the homogeneous dose at room temperature. Following irradiation, the samples were kept in a light-tight containment to reduce exposure from ambient light.

2.2. Samples characterization

2.2.1. Elemental analyses by EDX method

Elemental analyses of charcoal samples were carried out using a SEM-mounted Energy Dispersive X-ray (EDX) spectroscopy facility, which provide detailed information on the fractional weight of each element within the charcoal samples along with its composition. The parent Scanning Electron Microscopy (SEM) also being used to capture an image for the external morphology of the sample surface. Herein, a new generation Hitachi TM3030 Tabletop SEM (Japan) was used, operating at an accelerating voltage of 15 kV. This facility is accommodated in the University of Malaya's High Impact Research Central Facilities (HIR) building. EDX analysis generates data in the form of spectra with peaks corresponding to specific elements. EDX systems, which are commonly integrated into SEMs, include a sensitive x-ray detector, liquid nitrogen for cooling, and Quantax software for analysing energy spectra. Since x-rays are electromagnetic radiation, a modern detector known as silicon drift detectors is used because of its designed to function at higher x-ray count rates without the need for nitrogen liquid for cooling. The EDX detector contains a crystal capable of absorbing the energy of incoming x-rays through ionisation, producing free electrons that become conductive along with an electrical charge. The energy of individual X-rays is then converted by the X-ray detector into electrical pulses that correspond to the X-rays of the specific elements. A spectrum of X-ray counts vs energy (keV) will be displayed on the computer screen, along with the sample's elemental compositions.

2.2.2. Raman and Photoluminescence spectroscopy

The Raman spectroscopy analysis of the irradiated samples was performed using a Renishaw inViaTM system equipped with an Ar+ 532 nm excitation laser, with the energy of 2.33 eV and a laser beam spot diameter of <0.8 μm (assuming 1.22λ/NA, with 0.9 NA numerical aperture). The region of interest being examined using a 50 × objective lens to provide information on physical parameters relating to the defects participating in the luminescence process. The scattered light intensity was captured at a 90° angle to the excitation beam using a
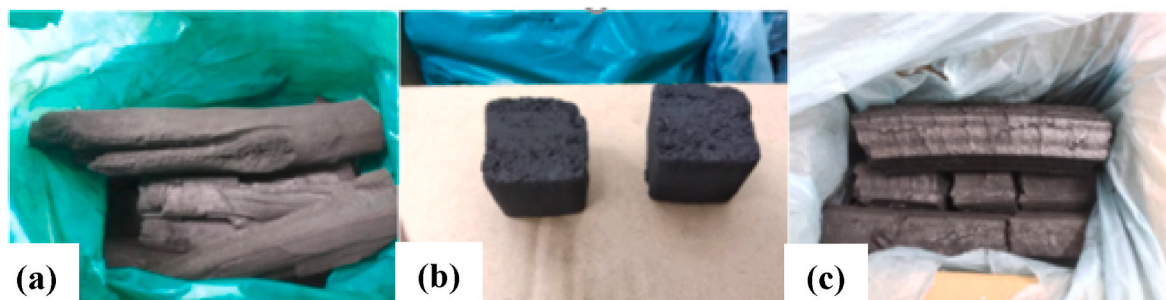
Fig. 1. Image of different types of commercially available charcoal; (a) Mangrove Charcoal, (b) Coconut Charcoal, and (c) Sawdust Charcoal. Similar manufacturer for all sample types were purchased from JS Resources Pte Ltd.

grating of 1800 lines/mm and detection with a 578 × 400-pixel Peltier-cooled charge-coupled system (CCD) camera.

Using the similar MicroRaman spectrometer, measurements of photoluminescence (PL) were obtained. The system was used with a 40 × objective lens, a grating system with 1200 lines/mm, and a laser at 325 nm for target excitation, with experience indicating that a higher excitation wavelength would result in a reduction in PL intensity (Bradley et al., 2021). Measurements were taken a few days after irradiation at room temperature, allowing for the identification of stable defect generation while also reducing the impact of thermal fading on the accuracy of TL yield estimation (Nawi et al., 2020).

2.2.3. X-ray diffraction analysis (XRD)

X-ray diffraction analysis (XRD) was performed to measure the crystal structure and structure parameters of all the charcoal samples using a Malvern PANalytical diffractometer, model Empyrean, equipped with a standard Ni-filtered Cu-Kα radiation (λ = 1.54056 A; Cu Ka1 8.04 keV x-rays), step size 0.026° in scanning mode, with 2 theta measurements from 10° to 80° at a scanning step time of 148 s, operated at 40 kV and 40 mA. In order to calculate the atomic spacing, the charcoal samples' characteristic XRD peak corresponding to the (002) plane was chosen (Bradley et al., 2020; Nawi et al., 2021).

3. Results and discussion

3.1. Elemental composition and effective atomic number (Z_{eff})

In order to provide information on photon interactions within targets, effective atomic number (Z_{eff}) and electron density are required, with Z_{eff} generally being considered the most useful parameter in accurately predicting absorbed dose since certain interactions are affected by the atomic number due to various types of photon interactions in a multi-elemental medium (Bradley et al., 2021). In current research, Z_{eff} of the different type of charcoal were estimated using the well-established so-called Mayneord Equation (1) (Khan and Gibbons, 2014):

$$Z_{eff} = (a_1 z_1^m + a_2 z_2^m + a_3 z_3^m + \dots \dots a_n z_n^m)^{1/m} \quad (1)$$

where a_1, $a_2 \dots a_n$, are the fractional contributions of each element to the total number of electrons in the mixture and m is equal to 2.94 being considered the best fit in taking account of the photoelectric dominating interaction. Table 1 displays the Z_{eff} of each charcoal samples investigated in current research. SEM–EDX analysis was being used to trace the relative distribution of carbon content in the samples, recognising the other elemental contributions including of oxygen, nitrogen, aluminium, and silica. Elemental distribution analysis was performed on each sample by measuring at three different points, which is detailed in Table 1 in terms of the mean fractional weight of each element within the various types of charcoal.

Photomicrograph of the sample is demonstrated in Fig. 2. The materials under investigation is expected to be heterogeneous, when viewed at the micron scale. For instance, EDX measurements were conducted at three points on the different forms of charcoal and Table 1

gives the averaged values obtained from the analysis. The morphology of the samples is quite different for mangrove, coconut and sawdust charcoals (SEM images Fig. 2), particularly for (a) the mangrove charcoal - where this might reflect imaging of a fragment with the graphitic layers viewed edge on (as opposed to face on). It is likely that there will be a variation in the relative amounts of graphitic carbon and amorphous carbon in the samples and this would vary according to the processing of the materials. Due to this, there would be a variation in that ratio between batches and, possibly, between samples from the same batch.

Table 1 shows that coconut charcoal has the highest carbon content, at 73.45%, followed by sawdust charcoal and mangrove charcoal, at 71.69% and 65.60%, respectively. However, non-carbon elemental data within the charcoal samples are particularly pertinent, oxygen being a considerable source of defects, with aluminium being a particularly well-known getter material, scavenging free oxygen (Bradley et al., 2021). Based on SEM-EDX values, the following equation (2) can be used to calculate the number of electrons per gram of samples:

$$N_e = \frac{N_A Z}{A_w}(W_i) \quad (2)$$

with N_A is the Avogadro number, A_w is the atomic weight and W_i is the fractional weight, and Z is the atomic weight of each individual element. By determining the number of electrons per gram, as in Equation (2), Z_{eff} can be evaluated via Equation (1). Therefore, the values of Z_{eff} for charcoal samples are found to range from 6.65 to 6.74 as shown in Table 1. It is preferable for a dosimeter to be soft tissue equivalent ($Z_{eff} = 7.46$) in clinical dosimetry to make sure response independence from incident photon energy, while the TLD-100 being particularly so with the Z_{eff} of 8.2 (Nawi et al., 2020). Thus, charcoal samples have the value of Z_{eff} not differing too greatly from that of human soft tissue.

3.2. Raman spectroscopy analysis

A novel method of dosimetry was established by use of Raman spectroscopy. Raman spectroscopic studies of carbonaceous materials are, until now, mainly devoted to geological and industrial materials. It is a very sensitive tool to study the carbon allotropes (Huong, 1991; Cataldo, 1999) and become a powerful, non-invasive method to characterize the presence of defects in the crystalline lattice of graphite, with the ability to analyse particles down to 1 μm and its non-destructiveness make it an ideal tool for pigments investigation (Elman et al., 1982; Niwase et al., 1990; Kitajima et al., 1987; Coccato et al., 2015). A large amount of information such as defects due to structural arrangements, sp^2 hybridization, interstitial gap, the luminescence/trapping centre due to presence of impurities in the graphite media can be studied from the Raman spectrum and their behaviour under varying physical conditions (Bradley et al., 2019; Abdul Sani et al., 2020; Nawi et al., 2020). The Raman Spectra generated corresponds directly to specific molecular bond vibrations such as C - C and C = C, with diamonds having one sharp peak at 1333 cm^{-1} and graphite having two strong peaks called the defect mode (D-peak) at 1350 cm^{-1} and graphite mode (G-peak) at

Table 1

Results using EDX analysis and effective atomic number for each different types of charcoal samples.

| Samples/Elements	Electronic configuration	Mangrove Charcoal		Coconut Charcoal		Sawdust Charcoal	
		Weight (%)	Atomic (%)	Weight (%)	Atomic (%)	Weight (%)	Atomic (%)
C	$1s^2 2s^2 2p^2$	65.60	71.17	73.45	78.14	71.69	76.58
O	$1s^2 2s^2 2p^4$	27.44	22.35	18.20	14.53	20.41	16.37
N	$1s^2 2s^2 2p^3$	6.96	6.47	7.71	7.04	7.51	6.88
Si	$1s^2 2s^2 2p^6 3s^2 3p^2$	NA	NA	0.54	0.25	0.32	0.15
Al	$1s^2 2s^2 2p^6 3s^2 3p^1$	NA	NA	0.10	0.05	0.06	0.03
Z_{eff}		**6.74**		**6.65**		**6.74**	

[a]NA = Not Available.
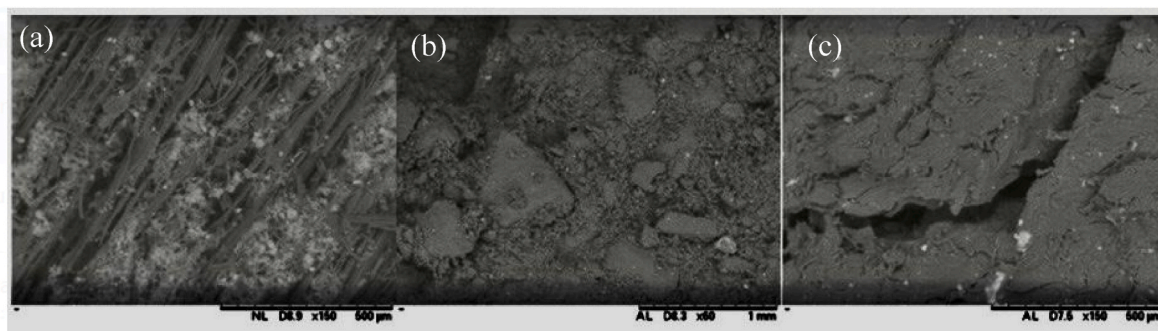
Fig. 2. SEM images of the samples of various type of charcoal; (a) Mangrove Charcoal (b) Coconut Charcoal, (c) Sawdust Charcoal for non-irradiated samples.

1580 cm^{-1}.

As a result, the Raman spectral profile is said to be the chemical fingerprint that is unique to the materials. Throughout the Raman analysis in the range of 1000–3000 cm^{-1}, all the Raman spectra for different types of charcoal samples within the dose range study, i.e., 0–10 Gy (see Fig. 3) demonstrate five peaks located at 1344 to 1352 cm^{-1}, 1581 to 1585 cm^{-1}, 1620 to 1625 cm^{-1}, 2702 to 2710 cm^{-1}, and 2943 to 2950 cm^{-1}, which are known as the D, G, D′, G′, and (D + D′) bands, respectively. Unlike the relatively narrow G′ band at 2700 cm^{-1} retrieved from Raman scattering of graphite materials in Bradley and co-workers investigate (Bradley et al., 2019; Abdul Sani et al., 2020; Nawi et al., 2020, 2021), the lack of a well-defined G′ band (particularly for coconut charcoal samples), as shown in Fig. 3, is most likely evidence of a second stage of amorphization, in which the nanocrystalline graphite has gradually become amorphous carbon (Ferrari and Robertson, 2000). Irrespective of the nature of carbon-rich material studied, including the

carbonaceous hair explored here, the two prominent bands with corresponding Raman shifts are very similar to the well-known D and G bands observed in the Raman spectra of disordered graphite, as well as the reported from several carbon-based research findings as shown in Table 2. Shift in the G and D bands in composites is attributed to an increase in electron-phonon interactions, which blueshifts and sharpens the G peak while broadening the D band. Generally, Raman bands shift due to intrinsic material and measurement setup properties (orientational effects, wavelength dependent band shift and intensity, etc.), as well as band overlap (Arora et al., 2014). G peak is relevant to the graphite E$_{2g}$ symmetry of the interlayer mode, reflecting the vibration of sp^2-hybridised carbon atoms in a two-dimensional hexagonal lattice. While D peak referred to induced by sp^3 electronic states which is defect in planar sp^2 graphitic structure was visualized. This peak is associated with the vibration of carbon atoms with disordered graphite, such as defects, dangling bonds in plane terminations and grain boundaries. The
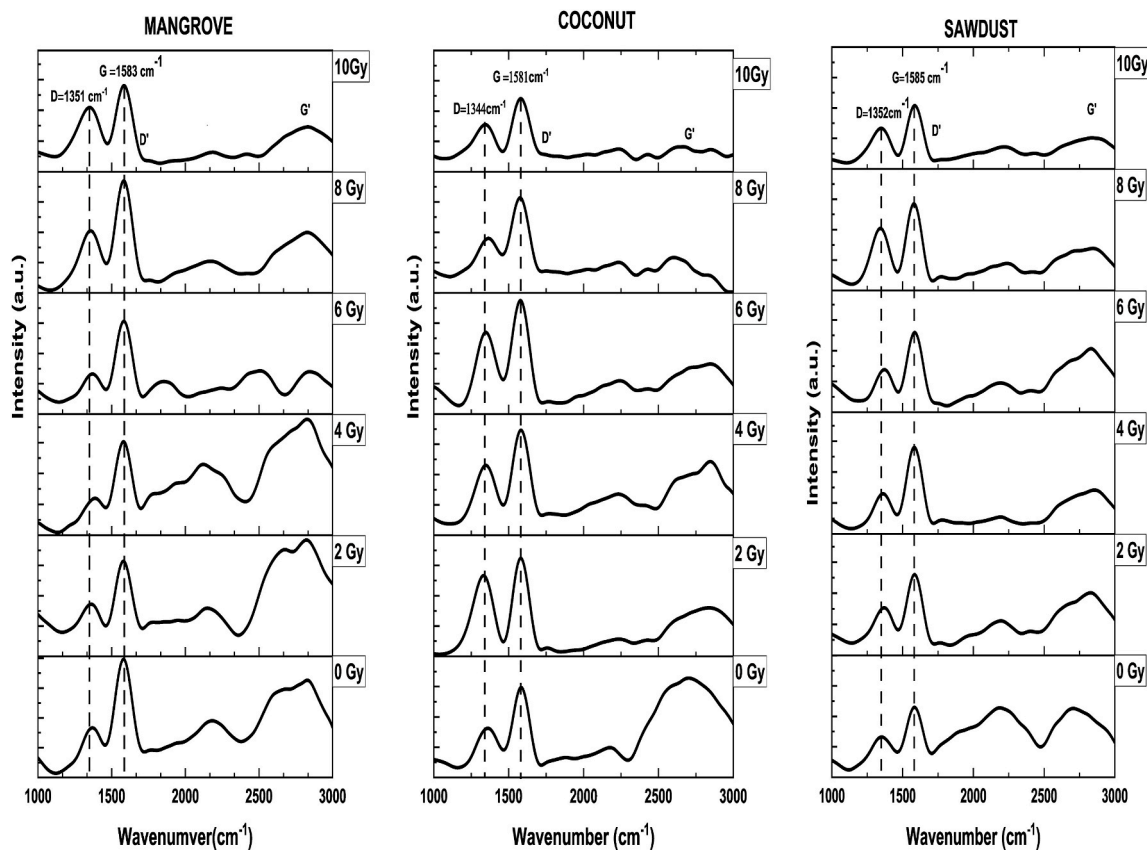

Fig. 3. Wide scale Raman Spectra of Mangrove charcoal, coconut charcoal and sawdust charcoal samples irradiated within the dose range 0–10 Gy of gamma irradiation.

Table 2

The Raman D- and G peak intensity of carbon-based materials as encountered in current study and previous research.

Authors	Carbon Materials	Type of ionizing radiation	Dose (Gy)	E_{laser} (eV)	D-peak (cm^{-1})	G-peak (cm^{-1})
Almugren et al., (current study)	Mangrove charcoal	Gamma-ray	0–10	2.33	~1351	~1583
	Coconut charcoal				~1344	~1581
	Sawdust charcoal				~1352	~1585
Bradley et al. (2019)	Pencils 8H and 2B	Gamma-ray	1–100	2.33	~1350	~1570
Abdul Sani et al. (2020)	Pencils H and 9B	Gamma-ray	0–20	2.41	~1348	~1578
Nawi et al. (2020)	Polymer pencil-lead graphite (PPLG) – (0.3 mm, 0.5 mm, 0.7 mm, and 0.9 mm diameter)	Gamma-ray	0–200	2.33	~1349	~1576
Nawi et al., 2021	Mechanical pencil lead 2B and HB - (0.3 mm diameter)	Neutron	0–200	2.33	~1345	~1576
Lam et., 2021	Hair	Gamma-ray	0.5–200	2.33	~1370	~1589
Bradley et al. (2021)	Graphite sheet	Gamma-ray	0.5–20	2.33	~1352	~1582

D peak is related to the double-resonance band, which was identified as a benchmark of structural disorder due to finite particle size (Hiura et al., 1993), graphite curvature effects, defects caused by pentagons or heptagons, and nanoscale or graphitic carbon particles on the tubes.

I_D and I_G were obtained from deconvoluted Raman spectra using OriginPro 2018 software; smoothing and baseline correction were applied to the raw Raman spectra prior to deconvolution, determining the ratio of peak intensity at the D and G bands (I_D/I_G) for each type of charcoal samples. D/G ratio relates to sp^3/sp^2 carbon ratio. If carbon material is fully oxidized, i.e., all carbons are sp^3. If D peak is higher, it means that the sp^2 bonds are broken which in turn means that there are more sp^3 bonds and more transition from sp^2 to sp^3 material, and there will be a maximum D/G ratio. As a result, the I_D/I_G ratio is frequently used to estimate the number and size of sp^2 clusters in carbon structures. Fig. 4 demonstrates the I_D/I_G intensity ratio as a function of irradiation dose for each type of charcoal samples irradiated from 0 to 10 Gy of gamma-ray. It is apparent that all the graph show a fluctuating pattern in respect of the I_D/I_G intensity ratio across the entire dose range study, showing a pattern familiar in prior investigations of carbon-rich materials such as pencil lead (Nawi et al., 2020, 2021), pyrolytic graphite (Abdul Sani et al., 2020), hair (Lam et al., 2021) and graphite sheet (Bradley et al., 2021). The observed oscillatory pattern of the Raman I_D/I_G ratio has previously also been reported by this group for a variety of graphitic materials, both for wave and particle irradiations, the range depending on the surface to volume ratio and linear energy transfer (LET). The oscillatory pattern is interpreted to result from a domination of either growth in defects generation or reduction in defects density due to internal irradiation-driven annealing.

The in-plane crystallite size values (L_a) were calculated using wavelength-corrected as in equation (3) by the Tuinstra-Koenig formula:

$$L_a \text{ (nm)} = (2.4 \times 10^{-10}) \, \lambda_{laser}^4 \, (I_D/I_G)^{-1} \tag{3}$$

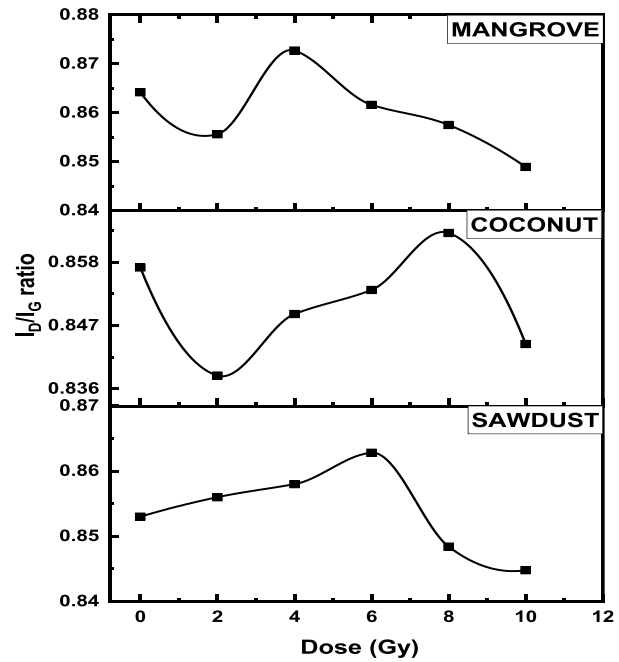**Fig. 4.** The Raman intensity ratio I_D/I_G for various type of charcoal samples irradiated using ^{60}Co γ-rays, irradiation dose covering the range 0–10 Gy.

where $\lambda_{Ar + laser} = 532$ nm. L_a values are affected by the microcrystalline boundary defect, which affects the electrical resistivity of crystallite graphite. Seeing as electrical resistivity is caused arising in part by carrier hopping between crystallites in the charcoal samples, increasing crystallite size reduces resistivity. Fig. 5 illustrates the intensities I_D/I_G ratio are inversely proportional to the crystallite sizes, $1/L_a$ for all types
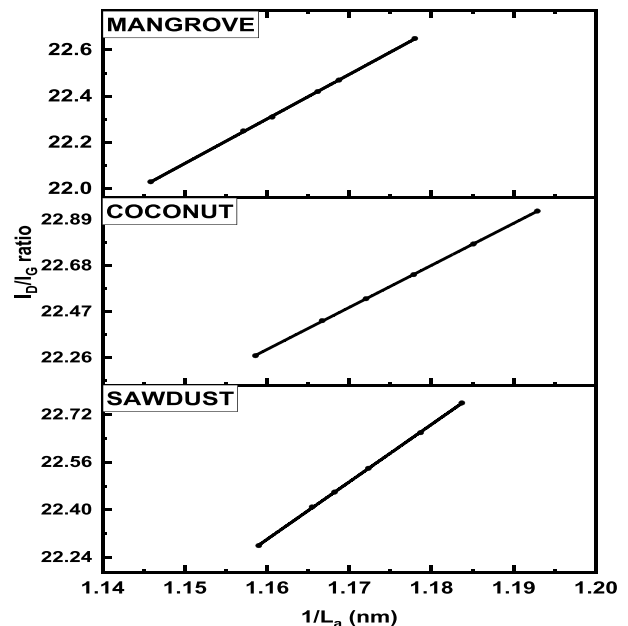

Fig. 5. The intensity ratio I_D/I_G against $1/L_a$ for difference types of charcoal, with I_D/I_G corresponding to ^{60}Co gamma ray doses from 0 to 10 Gy.

of charcoal samples at different radiation doses. This implies that the crystallite size is inversely related to the D-band. As a result, if radiation exposure creates more defects (D-band) in the material, the crystallite size of the material will eventually decrease (Table 3). In other words, increase in the defect density with respect to irradiation, in-plane crystallite size decreasing together with increment in D peak intensity, hence, the I_D/I_G is attributed to a particle size effect.

3.3. Photoluminescence (PL) spectroscopy analysis

Photoluminescence offers itself as a highly sensitive analytical tool in respect of the optical properties of carbon-based materials, including the present charcoal samples, being dependent on active centres, host structure, and interactions. In the case of photo–excitation, this luminescence is called photoluminescence. Thus photoluminescence is the spontaneous emission of light from a material under optical excitation. Photo excitation causes electrons within the material to move into permissible excited states. When these electrons return to their equilibrium states, the excess energy is released and may include the emission of light (a radiative process) or may not (a non-radiative process). The energy of the emitted light (photoluminescence) relates to the difference in energy levels between the two electron states involved in the transition between the excited state and the equilibrium state. The quantity of the emitted light is related to the relative contribution of the radiative process.

Due to unforeseen circumstances of restricted access to the laboratory facilities during the COVID-19 pandemic, only data on coconut charcoal samples (0–6 Gy) were obtained from the PL analysis for current study. Herein, two prominent peaks corresponding to absorption and emission can be seen in Fig. 6, encompassed within the range 400–1400 nm defined by the first and second peaks, respectively. The absorption peak was caused by laser photons with enough energy to cause photoexcitation, while the emission peak was caused by photoemission caused by electron-hole recombination. As the gamma dose increased, the PL spectra shifted to shorter wavelengths, resulting the ionizing radiation changes the optical spectra by trapping and releasing pairs of electrons and positive holes, as well as forming mediated defects that increase absorption and emission intensity, as predicted. The energy band gap, E_g is obtained from the peak of emission photon (second peak) of coconut charcoal samples were calculated using $E_g = hc/\lambda$, with h the Planck constant, c the speed of light and λ the corresponding wavelength based on PL spectra, and tabulated in Table 4, with the average of 1.111 ± 0.091 eV. A linear increase in band gap energy with increasing dose irradiation would be an ideal dose-response interpretation, because as the radiation dose increases, the defect energy states move to a deeper level, resulting in increased band gap energy. Nevertheless, as shown in Table 4, the band gap energy of the coconut samples fluctuates with increasing dose radiation, indicating a competition between irradiation-induced defects generation and self-repair processes, proven by plotting the graph of the maximum PL intensity of emission peak as the function of dose (see Fig. 7). The results, supportive of the Raman and XRD studies, are readily understood to arise from irradiation
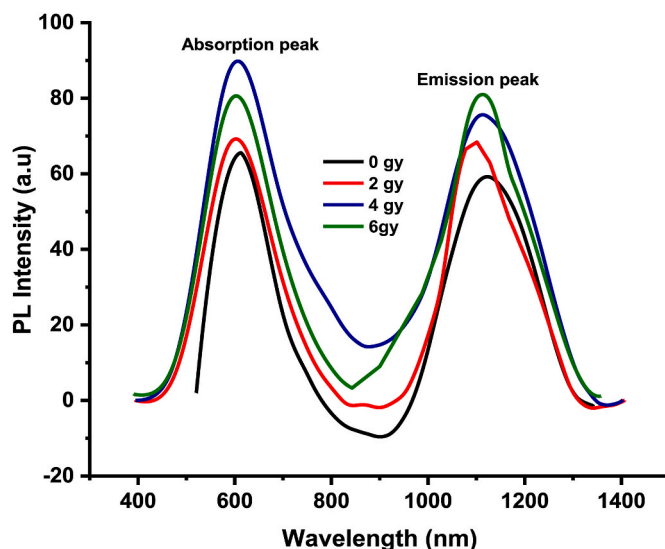
Table 3
Details of the I_D/I_G ratio and crystallite size, L_a, for various types of charcoal after gamma irradiation at doses ranging from 0 to 10 Gy.

Dose (Gy)	Mangrove Charcoal		Coconut charcoal		Sawdust charcoal	
	I_D/I_G ratio	Crystallite size, L_a (nm)	I_D/I_G ratio	Crystallite size, L_a (nm)	I_D/I_G ratio	Crystallite size, L_a (nm)
0	0.8489	22.65	0.8438	22.78	0.8448	22.76
2	0.8575	22.42	0.8631	22.27	0.8484	22.66
4	0.8618	22.31	0.8532	22.53	0.8628	22.28
6	0.8727	22.03	0.8490	22.64	0.8580	22.41
8	0.8556	22.47	0.8383	22.93	0.8560	22.46
10	0.8642	22.25	0.8571	22.43	0.8530	22.54

Fig. 6. PL spectra of coconut samples subjected to ^{60}Co gamma irradiation doses ranging from 0 to 6 Gy.

Table 4
The calculation of energy band gap of coconut charcoal samples from the emission peak within dose range study i.e., 0–6 Gy of ^{60}Co gamma irradiation.

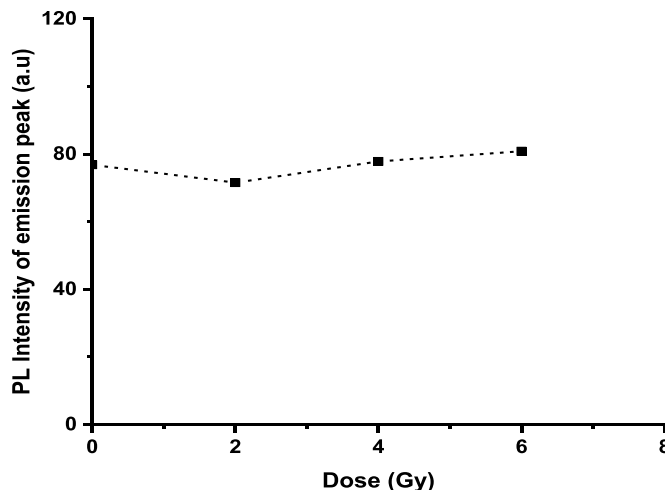| Dose (Gy)	Wavelength (nm)	Energy Bandgap (Ev)
0	1117.33	1.087 ± 0.4
2	1123.23	1.118 ± 0.2
4	1119.46	1.119 ± 0.5
6	1117.63	1.121 ± 0.1

Fig. 7. Maximum PL intensity extracted from the emission peaks of PL spectra, covering doses 0–6 Gy of ^{60}Co gamma irradiation.

changes occurring at the microscopic level. Regrettably, due to the limitations of our data and the dose range investigated, a linear dose-response for the coconut samples cannot be firmly established. To properly characterize the dose-response with PL analysis for the next study, data for dose ranges beyond 10 Gy must be collected for all charcoal samples.

3.4. X-ray diffraction (XRD) analysis

XRD patterns were used to investigate various types of charcoal

samples, which ranged from 10° to 80° at a scanning step time of 148 s at room temperature, as well as dose points ranging from 0 to 10 Gy. Fig. 8 (a), (b) and (c) show the respective XRD patterns, revealing shifts to greater angular value as a function of dose between 0 and 10 Gy. Across all scenarios for each charcoal samples, the findings are related to the particular Miller indices (002) and (100) graphite peaks, which are suggestive of natural graphite samples (Bradley et al., 2019). A phenomenon of XRD pattern previously found in an independent investigation by Pies et al. (2008) for carbonized wood in the form of Japanese Cedar charcoal materials. Graphite shows characteristic peak typically at around at $2\theta = 26.7°$ to 26.8° (Abdul Sani et al., 2020; Bradley et al., 2020), corresponding to the (002) plane is due to the mixture of amorphous and nanocrystalline phases (Xing et al., 2013). Herein, the Miller indices (002) were used to calculate the atomic spacing for mangrove, coconut, and sawdust charcoal, revealing the asymmetric shape of the (002) peaks at approximately $2\theta = 23.95°-24.26°$, 23.95°–24.29°, and 24.26°–25.71°, respectively (Fig. 8). Therefore, from the XRD spectra of the samples, the D-spacing (d) and the crystallite size (L_c) that correspond to the (002) plane was determined using Bragg's equation ($d_{002} = \lambda/2 \sin\theta$) with $\lambda = 1.54056$ and Scherrer equation ($L_c = K\lambda/\beta \cos\theta$) where $K = 0.9$ and β is the full-width at half-maximum of an acceptable Bragg line on standard 2θ scans, respectively. A smaller inter-layer spacing, d_{hkl}, and a larger crystalline size, L_c, in general, indicate a higher degree of structural order. Table 5 includes detailed estimations for the XRD structural parameters,

including the value of atomic spacing (d_{002}), average crystallite size, and FWHM of carbon-based charcoals. The changes in d_{002} and L_c parameter values in the mangrove, coconut, and sawdust charcoal samples reveal that the structural order of the charcoal samples alteration upon irradiation. In addition, also results show that the diffraction angle of the (002) line increases as the crystallize size increases, while the FWHM of the (002) line decreases, indicating that gamma radiation may have caused damage to the degree of structural order of each sample. The L_c of mangrove samples, for example, decreases with 2 Gy irradiation and increases with 4 Gy irradiation by 1.11 nm–1.35 nm, indicating structural order recovery and improvement. Across the dose range studied, similar fluctuating patterns can be seen in the coconut and sawdust charcoal samples, supportive of the Raman results reported earlier in this study. A detail explanation regarding this situation have been described in Bradley et al. (2022), graphite possesses the compulsive ability to self-repair, absorbing damage that could otherwise lead to dissipation and distortion. In this consideration, increasing in irradiation doses produces an equivalent increase in the density of gamma photons, consequently the prompt greater numbers of photoelectrons and recoil electrons produced through the Compton and photoelectric effect scattering respectively (Abdul Sani et al., 2020). These electrons may cause the displacement of carbon atoms in graphitic materials through hard ("knock-on") collisions and if the energies of the colliding electrons are larger than the threshold displacement energy of the material, collision cascade may also occur. Conventionally, the displacement of carbon
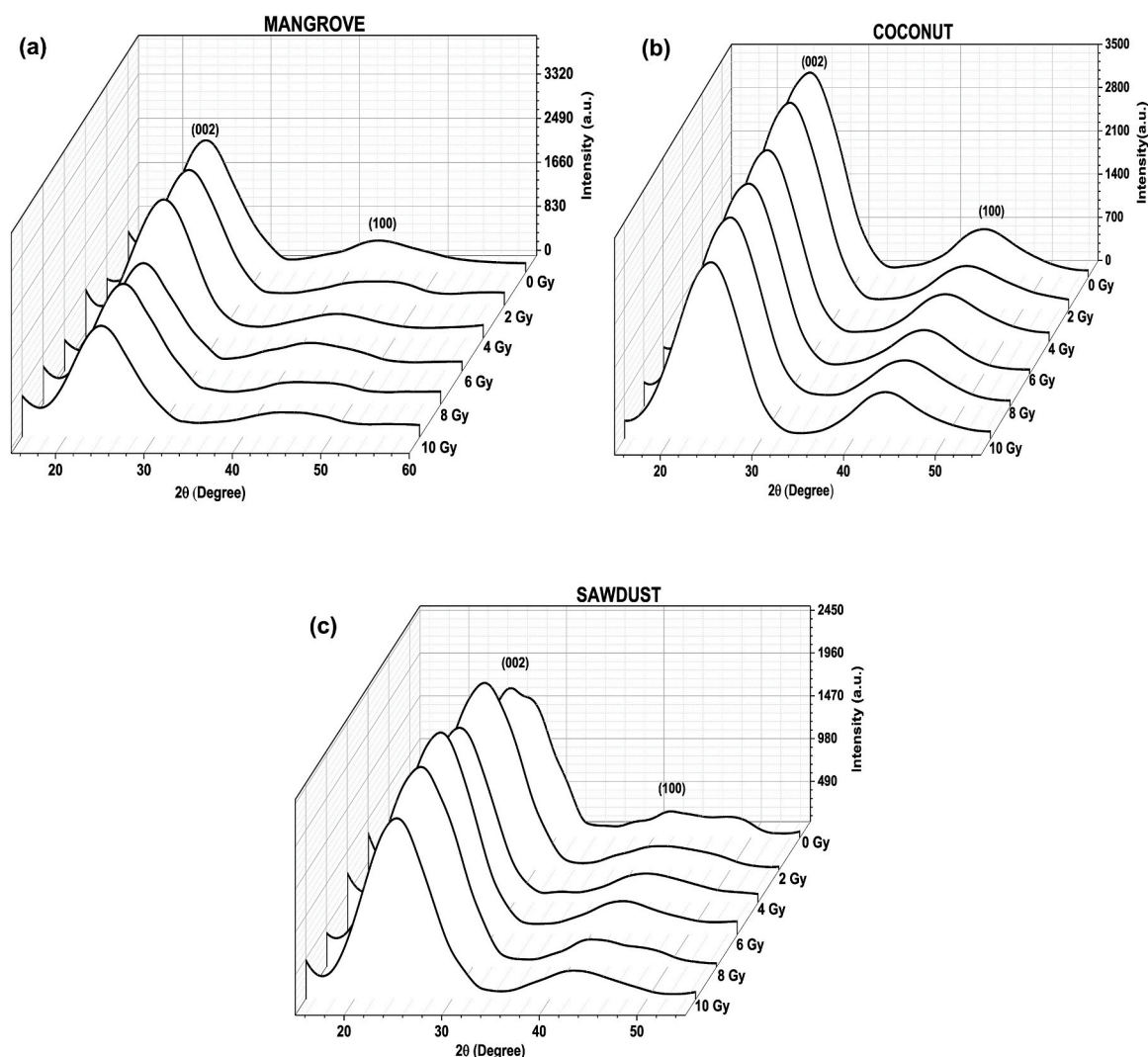

Fig. 8. XRD spectra for carbon-based charcoal; (a) Mangrove, (b) Coconut and (c) Sawdust samples, irradiated to gamma entrance doses from 0 to 10 Gy.

Table 5

XRD structural parameters of Magrove charcoal, Coconut charcoal, and Sawdust charcoal samples at different irradiation dose.

Mangrove charcoal				
Dose (Gy)	2θ (°)	d_{002} (nm)	$FWHM_{002}$ (°)	L_c (002) (nm)
0	23.95	0.3713	7.801	1.28
2	24.26	0.3667	8.228	1.11
4	23.74	0.3745	8.011	1.35
6	24.13	0.3686	6.581	1.44
8	24.23	0.3670	7.077	1.30
10	24.05	0.3697	6.928	1.40
Coconut charcoal				
Dose (Gy)	2θ (°)	d_{002} (nm)	$FWHM_{002}$ (°)	L_c (002) (nm)
0	24.28	0.3678	8.269	1.13
2	24.39	0.3662	8.259	1.10
4	23.99	0.3707	7.946	1.25
6	23.95	0.3711	8.450	1.19
8	24.14	0.3684	8.091	1.17
10	24.15	0.3682	7.973	1.18
Sawdust charcoal				
Dose (Gy)	2θ (°)	d_{002} (nm)	$FWHM_{002}$ (°)	L_c (002) (nm)
0	25.71	0.3659	7.763	1.17
2	24.65	0.3625	8.738	0.95
4	24.26	0.3666	8.312	1.10
6	24.27	0.3665	8.312	1.10
8	24.54	0.3625	9.214	0.95
10	24.30	0.3659	7.763	1.17

atoms from their lattice sites will break the C–C bonds, producing dangling bonds (immobilized free radical) and Frenkel defects, which in turn increases the structural disorder of the material. However as mentioned by Bradley et al. (2020) and Ding et al. (2007), graphite possesses a self-repairing mechanism that allows higher energy defects such as vacancies and holes to be avoided. Thus, the vacancies caused by irradiation can be repaired by dangling bond saturation and forming non-hexagonal rings accordingly (Li et al., 2013). It was also theorized by Telling et al. (2003) that graphite vacancy defects in graphite could be stabilized through the formation of complexes over the large inter-layer distance.

4. Conclusion

The present investigation has been concerned on the microstructure and defects of commercial charcoal from three different types: mangrove, coconut, and green charcoal recycled from sawdust, working with photon-mediated interactions at radiotherapy dose levels, as a fine medium with a low atomic number for radiation dosimetry. According to the Mayneord formula, the three types of charcoal have Z_{eff} values ranging from 6.65 to 6.74, which is close to the value reported for human soft tissues, which is at $Z_{eff} = 7.4$, making charcoal (particularly mangrove and sawdust at $Z_{eff} = 6.74$) a promising potential candidate as a dosimetric material. In addition, various types of charcoal were investigated via use of Raman, PL spectroscopy and XRD techniques, as several state-of-the-art methods so-called well-positioned defect-dependent analytical techniques to examine the change in elemental and structural characterization of the carbon-based samples. The outcomes for Raman, PL and XRD are seen to be supportive of one another, their response towards irradiation changes being readily understood at the microscopic level. Significant structural modifications were found at the given doses, manifest changes occurring in the shape and intensity of Raman spectra, showing the fluctuations in the structural order of the samples reflect the structural order-disorder competition of the samples upon irradiation. According to semiconductor-like behaviour, PL measurements produce prominent absorption and emission peaks, with the resulting mean E_g being found to be 1.111 ± 0.091 eV. It is worth noting, however, that the PL intensity peaks of coconut charcoal

demonstrated an increasing trend over the investigated dose range of 0–6 Gy. Notwithstanding, due to the limitations of the available data, we are unable to establish a firm linear dose-response relationship, and detail investigations at higher doses are required for further evaluations. From the XRD results, all samples show that the diffraction angle of the (002) line increases as the crystallize size increases, while the FWHM of the (002) line decreases, indicating that gamma radiation may have caused damage to the degree of structural order of each sample. As a result, all the techniques used in this study were discovered to be mutually beneficial.

Author statement

K.S. Almugren, designs the study and analysed the data. S.F. Abdul Sani, designs the study and analysed the data, revised the manuscript written by S.N. Mat Nawi. Irzwan Affendy Sulong, carried out the experimental work, participated in sample preparation and data collection, and drafted the manuscript. S. N. Mat Nawi, writes the manuscript and analysed the data. A.S. Siti Shafiqah, visualization the research work. D.A. Bradley, reviewing and editing the manuscript. All authors read and approved the final manuscript.

Declaration of competing interest

The authors declare that they have no known competing financial interests or personal relationships that could have appeared to influence the work reported in this paper.

References

Abdul Sani, S.F., Ismail, S.S., Almugren, K.S., Khandaker, M.U., Bradley, D.A., 2020. Dosimetric utility of structural changes in gamma irradiated graphite-rich pencils. Radiat. Phys. Chem., 108703 https://doi.org/10.1016/j.radphyschem.2020.108703.

Arora, M., Wahab, M.A., Saini, P., 2014. Permittivity and electromagnetic interference shielding investigations of activated charcoal loaded acrylic coating compositions. Polym. Mater.

Bradley, D.A., Rozaila, Z.S., Khandaker, M.U., Almugren, K.S., Meevasana, W., Sani, S.A., 2019. Raman spectroscopy and X-ray photo-spectroscopy analysis of graphite media irradiated at low doses. Appl. Radiat. Isot. 147, 105–112. https://doi.org/10.1016/j.apradiso.2019.02.016.

Bradley, D.A., Mat Nawi, S.N., Khandaker, M.U., Almugren, K.S., Abdul Sani, S.F., 2020. Sub kGy photon irradiation alterations in graphite. Appl. Radiat. Isot. 161, 109168.

Bradley, D.A., Ee, L.S., Nawi, S.N.M., Sani, S.F.A., Khandaker, M., Alzimami, K., Jambi, L., 2021. Graphite sheets in study of radiation dosimetry and associated investigations of damage. Appl. Radiat. Isot. 174, 109769.

Bradley, D.A., Ee, L.S., Nawi, S.N.M., Sani, S.F.A., Khandaker, M., Alzimami, K., Jambi, L., Alqhatani, A., 2022. Radiation induced defects in graphite. Appl. Radiat. Isot., 110141

Brooks, J.K., Bashirelahi, N., Reynolds, M.A., 2017. Charcoal and charcoal-based dentifrices: a literature review. J. Am. Dent. Assoc. 148 (9), 661–670.

Cataldo, F., 1999 Jan 1. Spectroscopical characterization of carbonaceous matter prepared through the Glaser coupling reaction route. Carbon 37 (1), 161–163. https://doi.org/10.1016/S0008-6223(98)90106-3.

Coccato, A., Jehlicka, J., Moens, L., Vandenabeele, P., 2015. Raman spectroscopy for the investigation of carbon-based black pigments. J. Raman Spectrosc. 46 (10), 1003–1015.

Ding, F., Jiao, K., Lin, Y., Yakobson, B.I., 2007. How evaporating carbon nanotubes retain their perfection? Nano Lett. 7 (3), 681–684.

Elman, B.S., Shayegan, M., Dresselhaus, M.S., Mazurek, H., Dresselhaus, G., 1982 Mar 15. Structural characterization of ion-implanted graphite. Phys. Rev. B 25 (6), 4142. https://doi.org/10.1103/PhysRevB.25.4142.

Ferrari, A.C., Robertson, J., 2000. Interpretation of Raman spectra of disordered and amorphous carbon. Phys. Rev. B 61, 14095–14107.

Hiura, H., Ebbesen, T.W., Tanigaki, K., Takahashi, H., 1993 Feb 5. Raman studies of carbon nanotubes. Chem. Phys. Lett. 202 (6), 509–512. https://doi.org/10.1016/0009-2614(93)90040-8.

Huong, P.V., 1991 Aug 15. Structural studies of diamond films and ultrahard materials by Raman and micro-Raman spectroscopies. Diam. Relat. Mater. 1 (1), 33–41. https://doi.org/10.1016/0925-9635(91)90009-Y.

Khan, F.M., Gibbons, J.P., 2014. Khan's the Physics of Radiation Therapy. Lippincott Williams & Wilkins.

Kitajima, M., Okada, M., Aoki, K., 1987. Observation of shape change in the Raman spectrum of graphite exposed to deuterium glow. J. Nucl. Mater. 149 (2), 269–271. https://doi.org/10.1016/0022-3115(87)90487-9.

Lam, S.E., Nawi, S.N.M., Sani, S.F.A., Khandaker, M.U., Bradley, D.A., 2021. Raman and photoluminescence spectroscopy analysis of gamma irradiated human hair. Sci. Rep. 11 (1), 1–10.

Li, B., Feng, Y., Ding, K., Qian, G., Zhang, X., Zhang, J., 2013. The effect of gamma ray irradiation on the structure of graphite and multi-walled carbon nanotubes. Carbon 60, 186–192.

Nawi, S.N.M., Khandaker, M.U., Bradley, D.A., Sani, S.A., Almugren, K.S., Sulieman, A., 2020. Polymer pencil lead graphite for in vivo radiation dosimetry. Diam. Relat. Mater., 107860 https://doi.org/10.1016/j.diamond.2020.107860.

Nawi, S.N.M., Khandaker, M.U., Sani, S.A., Ismail, S.S., Al-Mugren, K.S., Islam, M.A., Bradley, D.A., 2021a. Structural and dosimetric study of sub-kGy neutron-irradiated graphitic media. Radiat. Phys. Chem. 189, 109709.

Nawi, S.N.M., Khandaker, M.U., Bradley, D.A., Sani, S.A., Al-mugren, K.S., 2021b. Characterization of a promising luminescence-based graphite radiation dosimeter. Radiat. Phys. Chem. 188, 109663.

Niwase, K., Nakamura, K., Shikama, T., Tanabe, T., 1990. On the amorphization of neutron-irradiated graphite. J. Nucl. Mater. 170 (1), 106–108. https://doi.org/10.1016/0022-3115(90)90332-H.

Pies, C., Hoffmann, B., Petrowsky, J., Yang, Y., Ternes, T.A., Hofmann, T., 2008. Characterization and source identification of polycyclic aromatic hydrocarbons (pahs) in river bank soils. Chemosphere 72 (10), 1594–160.

Telling, R.H., Ewels, C.P., Ahlam, A., Heggie, M.I., 2003. Wigner defects bridge the graphite gap. Nat. Mater. 2 (5), 333–337.

Xing, T., Li, L.H., Hou, L., Hu, X., Zhou, S., Peter, R., Chen, Y., 2013. Disorder in ball-milled graphite revealed by Raman spectroscopy. Carbon 57, 515–519.